Effect of CO_2 on oxy-fuel combustion of coal-char particles in a fluidized bed: modeling and comparison with the conventional mode of combustion

Changsheng Bu[a,b]*, Alberto Gómez–Barea[c], Xiaoping Chen[b]*,

Bo Leckner[d], Daoyin Liu[b], David Pallarès[d], Ping Lu[a]

a Jiangsu Provincial Key Laboratory of Materials Cycling and Pollution Control, School of Energy & Mechanical Engineering, Nanjing Normal University, Nanjing 210042, China
b Key Laboratory of Energy Thermal Conversion and Control of Ministry of Education, Southeast University, Nanjing, 210096, China.
c Chemical and Environmental Engineering Department, University of Seville, Seville 41092, Spain
d Department of Energy and Environment, Chalmers University of Technology, Göteborg 41296, Sweden

Abstract

A char combustion model is developed to study the effect of CO_2 on the combustion of coarse char particles under oxy−fuel conditions in a fluidized bed (FB). It is a transient one−dimensional model, taking into account the heat and mass transfer from the bed to the particle and the heterogeneous combustion and gasification of char. The model shows good ability to predict the char temperature history measured in our previous work for different combinations of O_2/CO_2 and O_2/N_2 with various coal types. Simulations are carried out to establish the role of CO_2 in oxy-fuel conversion at different O_2 levels, particle sizes, and bed temperatures. The model is used to analyze the relative contribution of carbon in the char consumed by CO_2 (gasification) and O_2 (combustion), as well as the differences of the peak temperatures and the burnout times in O_2/CO_2 and O_2/N_2 for char particles in a commercial FB combustor. The results indicate that the conversion of coarse (mm size) char particles in an oxy-FB is controlled by the diffusion of O_2 both in the O_2/CO_2 and O_2/N_2 case. The burn−out time decreases with the bed temperature also in both cases.. The lower O_2 diffusion rate in CO_2 compared to N_2, is the main reason for the longer burnout time and lower peak temperature found using O_2/CO_2 at bed temperatures of 1073-1173 K. In that temperature window, the contribution of the CO_2 –char gasification is limited, being notable only at high bed temperature in O_2/CO_2, e.g. 1223 K. In such high temperature conditions (rarely expected to be found in commercial coal FBC) the predicted burnout time of a lignite char-particle becomes shorter in O_2/CO_2 than in O_2/N_2.

Keywords: oxy–combustion; fluidized bed; modeling; char; coal; gasification

Nomenclature

Notations

Ar	Archimedes number,-
A_{CO/CO_2}	pre−exponential factor in Eq. (15),-
A_{kin}	pre−exponential factor for kinetic reaction of char,-
c_p	specific heat at constant pressure, $kJ/(kg \cdot K)$
E_{CO/CO_2}	activation energy in Eq. (15), kJ/mol
E_{kin}	activation energy for kinetic reaction of char, kJ/mol
d	diameter, m
D	molecular diffusivity, m^2/s
h_h	heat transfer coefficient, $W/(m^2 \cdot K)$
h_m	mass transfer coefficient, m/s
k_{kin}	kinetic reactivity of heterogeneous reaction, $kg/(m^2 \cdot s)$
M	molecular mass, mol/kg
Nu	Nusselt number,-
Pr	Prandtl number,-
r	distance from the particle' s center, m
R	radius of fuel particle, m
R_g	gas constant, $8.315 \times 10^{-3} kJ/(mol \cdot K)$
$\Re_v$	reaction rate, $kg/(m^3 \cdot s)$
s	specific surface area, m^2/m^3
S	source term in Eqs. (1) and (2), $kg/(m^3 \cdot s)$
Sc	Schmidt number,-
Sh	Sherwood number,-
t	time, s
T	temperature, K
u_f	fluidizing velocity, m/s
X_C	carbon conversion of the particle, -
x_C	local carbon conversion at an internal position of the particle, -
X_{gas}	percentage contribution of gasification to the consumption of char, %

Y	mass fraction, -

Greek letters

α	thermal diffusivity or mechanism coefficient of char combustion, m^2/s or -
β	mechanism coefficient of char combustion, -
δ	thicknesses of gas−film, m
ε	porosity, or bed voidage,-
λ	thermal conductivity, $W/(m \cdot K)$
ΔH	heat of chemical reaction, J/kg
ρ	density, kg/m^3
σ	Stephan−Boltzmann constant, $5.67\times10^{-8}\ W/(m^2 \cdot K^4)$
ϕ	mechanism factor of char combustion,-
ω	effective emissivity of the radiative exchange between bed and char particle,-

Subscripts

a	ash
b	bed materials or bed particle
$burn$	burnout
c	char
$conv$	convection
eff	effective
g	gas
h	heat
i,k	component:1−O_2, 2−CO_2, 3−CO, 4−N_2
j	heterogeneous reaction: 1−combustion, 2−gasification
m	mass
mf	under minimum fluidization conditions
p	char particle

$peak$	maximum
rad	radiation
s	particle surface
tot	total
0	initial value
∞	under bulk conditions

Important abbreviations

AC	Anthracite coal
BC	Bituminous coal
FB	Fluidized bed
LC	Lignite coal
SBC	Sub−bituminous coal

1. Introduction

Oxy−fuel combustion is considered one of the promising technologies to capture carbon dioxide from coal–fired power plants. In this technology, air (O_2/N_2) is substituted by pure oxygen mixed with recycled flue gas (mainly consisting of CO_2) before injection into a combustor. The formed flue gas with high CO_2 concentration could be compressed for utilization or storage. Thus, the primary difference between air combustion and oxy-fuel combustion is the high CO_2 level in oxy-fuel atmosphere as a result of replacing of N_2 with CO_2. Recently, many investigations have been carried out to understand the effect of the high CO_2 level on the combustion characteristics of pulverized coal (PC) [1]−[6]. The results indicate that the fuel-particle temperature drops 100−200 K and that gasification accounts for 8−20% of the carbon consumption at O_2 concentrations in O_2/CO_2 identical to those in O_2/N_2 [3][5]. This behavior is a consequence of the low diffusivity of O_2 in CO_2 and the large endothermicity of the CO_2-char reaction.

Oxy−fuel combustion of char in fluidized bed (FB) could differ from PC because of the larger particle size and the lower furnace temperature. Fundamental research about oxy−fuel combustion of coal particles in FB is scarce [7], in spite of the operation of pilot−scale FBs [8][9]. Brix et al. [10] studied millimeter-sized coal char in a laboratory−scale fixed bed at 1073 K in O_2/CO_2 and O_2/N_2 with 5−80 $\%_{vol}$ O_2 concentrations, and indicated

that the maximum char particle temperature decreases by 25–50 K in O_2/CO_2 as compared with that in O_2/N_2. Roy and Bhattacharya [11] studied oxy-fuel combustion of single coal-char particles in an FB reactor at 1153-1198 K with 5-15 $\%_{vol}$ O_2 concentrations. The combustion rate of char particle was found to increase with increasing bed temperature and O_2 concentration. In our previous work [12][13], devolatilization and char combustion of different ranks of coarse coal particles, including anthracite coal (AC), sub-bituminous coal (SBC), bituminous coal (BC), and lignite coal (LC), were experimentally examined in O_2/N_2 and O_2/CO_2 with 10−40 $\%_{vol}$ O_2 concentrations in an FB at 1088 K. In each test, a single coal particle was fed into the FB to ensure a uniform temperature and gas concentration around the fuel particle to accurately analyze its conversion behavior. Measurements showed that the devolatilization characteristics do not change much, but the char burnout time is prolonged and the peak temperature is lower when O_2/N_2 is replaced by O_2/CO_2 as a result of the low diffusivity of O_2 and the gasification reaction in O_2/CO_2. However, up to now, the quantitative effect of these factors on oxy-fuel FB combustion of char particles remains unclear.

Several particle-scale reaction models of fuel particles have been developed for the understanding of the combustion characteristics of a fuel particle in FB under conventional conditions, including zero and one dimensional transient models [14]-[15]. The main aim of the present work is to quantitatively examine the effect of CO_2 in oxy-fuel combustion of char particles in FB, including the changed diffusivity of O_2 and the occurrence of CO_2 gasification. It is considered that the size of coal-char particles used in the fluidized bed is large enough for the formation of heat and mass gradients inside a particle. A one-dimensional transient char combustion model is developed to describe the oxy-fuel combustion of a char particle in FB, implemented as a continuation of our already built model for coal devolatilization [16].The char combustion model accounts for mass and heat transfer in the gas boundary-layer during reaction (combustion and gasification) and within the char particle. The model is validated firstly by comparing simulations with the experimental results measured previously [13] and other reported data under different FB combustion conditions [17]-[20]. The model is then used to analyze the experimental data and clarify the effects of the low diffusivity of O_2 and the gasification reaction on the char conversion.

In addition, the FB boilers concerned could have an inlet oxygen concentration suitable for replacing air in an existing air-fired boiler (which would be a moderately higher than 21%, typically 30-35%, to compensate for the different properties of N_2 and CO_2 [13]), or the oxygen concentration could be much higher, intended for a newly designed boiler [21]. In both cases, the excess oxygen might not differ much from the conventional

value 3-4%, meaning that a fuel particle might meet a high oxygen concentration initially, but during most of its stay in the furnace the oxygen concentration would be lower than the inlet one. The model is also used to simulate the char combustion process at various O_2 levels, different particle sizes and bed temperatures, which cover the typical operation conditions of an FB boiler, and to explain the difference between conventional and oxy-fuel combustion.

2. Modeling approach

According to the evolution of the surface temperatures of the particle measured by the thermocouple, the particle did not collapse before the burnout of carbon [13]. In the present work, six conservation equations inside the fuel particle, energy, total mass, and mass fractions of O_2, CO_2, CO, and N_2, are taken into account to develop a one−dimensional, transient, char-combustion model. The interior and the exterior of the particle are connected by the boundary conditions at the particle' s surface. To handle the problem analytically, the assumptions made are summarized as follows:

(i) The geometry of the fuel particle is spherical;

(ii) The shape or dimensions of the particle do not change during its conversion;

(iii) The porosity, thermal conductivity, and heat capacity of the char particle change proportional to the degree of carbon conversion;

(iv) Initially, the pore space of the particle is filled with N_2 (in O_2/N_2) or CO_2 (in O_2/CO_2). The gases behave as ideal gases;

(v) The impact of the Knudsen effect on the diffusion coefficients is assumed negligible [22].

2.1 Transport equations

The conversion of the mass fraction of each component (i) inside the particle is,

$$\frac{\partial \varepsilon_p \rho_g Y_i}{\partial t} = \frac{1}{r^2}\frac{\partial}{\partial r}\left(r^2 \varepsilon_p \rho_g D_{eff,i}\frac{\partial Y_i}{\partial r}\right) + S_{m,i} \quad (1)$$

The heat conservation of the char particle is given as,

$$\frac{\partial((1-\varepsilon_p)\rho_p c_p T_p)}{\partial t} = \frac{1}{r^2}\frac{\partial}{\partial r}\left(\lambda_p r^2 \frac{\partial T_p}{\partial r}\right) + \sum S_{h,j} \quad (2)$$

The conservation of carbon in the char is given by,

$$\frac{\partial \rho_p}{\partial t} = -\sum \Re_{v,j} \quad (3)$$

The source terms in Eqs. (1) and (2) are the consumption and the generation of gas and the enthalpy of the chemical reactions in the char particle, respectively. The modeling of these two source terms is presented in Section 2.2.

The initial conditions of the fuel particle are,

$$at\ t = 0:\ \ 0 \le \mathrm{r} \le \mathrm{R},\ \mathrm{T_p} = \mathrm{T_0},\ \rho_p = \rho_{p,0},\ \varepsilon_p = \varepsilon_{p,0} \tag{4}$$

Because of symmetry at the center of the particle,

$$at\ r = 0:\ \ \left.\frac{\partial Y_i}{\partial r}\right|_{r=0} = \left.\frac{\partial T}{\partial r}\right|_{r=0} = 0 \tag{5}$$

At the particle surface, the mass and heat transfer between the particle and the bed are interpreted by,

$$at\ r = R:\ -D_i \left.\frac{\partial Y_i}{\partial \mathrm{r}}\right|_{r=R} = h_{m,i}\left(Y_{i,s} - Y_{i,\infty}\right) \tag{6}$$

$$at\ r = R:\ -\lambda_\mathrm{p} \left.\frac{\partial \mathrm{T_{ps}}}{\partial \mathrm{r}}\right|_{r=R} = \mathrm{h_{h,tot}}\left(\mathrm{T_{ps}} - \mathrm{T_b}\right) \tag{7}$$

Moreover, the sum of the mass fractions of all species inside the char particle should be unity,

$$\sum Y_i = 1 \tag{8}$$

The effective diffusivity of the gas species in the solid is estimated, considering the influence of the porous structure of the particle [23][24],

$$D_{eff,i} = \frac{\varepsilon_p}{\tau} D_i \approx \varepsilon_p^2\, D_i \tag{9}$$

Here, D_i is the pseudo-diffusion coefficient of species i in the gas mixture, calculated from the binary diffusion coefficients D_{ik} as [25],

$$D_i = (1 - Y_i) / \sum_{k \neq i}^{N} (X_k / D_{ik}) \tag{10}$$

In FB, the char particle is exposed to a surrounding of hot inert bed material, whose particles are smaller than those of char. The maximum values of the empirical relationships proposed by Palchonok [25] give the heat ($h_{h,conv}$) and mass ($\mathrm{h_m}$) transfer coefficients of the active particle, whose size is much larger than that of the inert bed particle in line with the experimental conditions used in the presented work.

$$Nu_b = h_{h,conv}\, d_b / \lambda_g = 0.85 Ar_b^{0.19} + 0.006 Ar_b^{0.5} Pr^{0.3} \tag{11}$$

$$Sh_{b,i} = h_{m,i}\, d_b / D_i = 0.09 Ar_b^{0.5} Sc^{0.3} \tag{12}$$

Where, Ar_b is the Archimedes number of inert (bed) particles, $\mathrm{Ar}_b = g d_b^3 \left(\rho_b - \rho_g\right) / \left(\nu_g^3 \rho_g\right)$.

The total heat transfer coefficient ($\mathrm{h_{h,tot}}$) includes the components of convective and radiative heat transfer,

$$\mathrm{h_{h,tot}} = \mathrm{h_{h,conv}} + \mathrm{h_{rad}} \tag{13}$$

$$h_{rad} = \sigma\omega\left(T_{ps} + T_b\right)\left(T_{ps}^2 + T_b^2\right) \quad (14)$$

2.2 Kinetics of the heterogeneous reactions

The char is assumed to be converted by CO_2 (gasification) and O_2 (combustion) simultaneously [3][6][26] so the following heterogeneous reactions are considered,

$$\frac{2(\alpha+\beta)}{\alpha+2\beta} C_{(s)} + O_2 \rightarrow \frac{2\alpha}{\alpha+2\beta} CO + \frac{2\beta}{\alpha+2\beta} CO_2 \quad \text{(Reaction 1)}$$

$$C_{(s)} + CO_2 \rightarrow 2CO \quad \text{(Reaction 2)}$$

The homogeneous reaction of CO, taking place outside of the particle, is not considered in the present model. Reaction 1 is exothermic, whereas Reaction 2 is endothermic. α and β are mechanism coefficients: $\alpha = 0$ means that CO_2 is the primary product of combustion, whereas CO is the primary combustion product when $\beta = 0$ [27]. Arthur [28] proposed a kinetic equation to estimate the produced ratio of CO/CO_2, which has been commonly used in modeling of the combustion of char particles [3][29],

$$\frac{\alpha}{\beta} = A_{CO/CO_2} \exp\left(-\frac{E_{CO/CO_2}}{R_g T_p}\right) \quad (15)$$

Reaction 2 accounts for the effect of CO_2 gasification on the conversion of the char particle, which is one of the main objectives studied in the present work.

The rates of the combustion and gasification reactions are modeled as global reactions [22][30],

$$\Re_{v,1} = \frac{2(\alpha+\beta)}{\alpha+2\beta} \cdot A_{kin,1} exp\left(-\frac{E_{kin,1}}{R_g T_p}\right) \cdot s \cdot Y_{O_2} \quad (16)$$

$$\Re_{v,2} = A_{kin,2} exp\left(-\frac{E_{kin,2}}{R_g T_p}\right) \cdot s \cdot Y_{CO_2} \quad (17)$$

In Eqs. (16) and (17), s is the available specific surface area, changing with the degree of local carbon conversion (x_C) and assumed to follow the random pore model [31]. The available specific surface area at zero carbon burn-off is s_0.

$$s = s_0(1 - x_C)\sqrt{1 - \Psi \ln(1 - x_C)} \quad (18)$$

Where, $x_C = 1 - m/m_0$, m_0 and m are the mass of carbon contained at initial time t_0 and time t. Ψ is a structural parameter, obtained by fitting experimental results, yielding various values of Ψ from 0.2 to 10 for different types of char. Here, the average value of 2.5 is selected for the different chars, as recommended in Refs. [32]-[33].

The corresponding source term (S_i) in Eq. (1) of each species during the conversion of a char particle can be calculated for the gas species, $i = 1(O_2)$, $i = 2(CO_2)$, $i = 3(CO)$, and $i = 4(N_2)$,

$$S_{m,1} = -\frac{M_1}{M_C}\Re_{v,1} \tag{19}$$

$$S_{m,2} = \frac{M_2}{M_C}\left(\frac{2\beta}{\alpha+2\beta}\Re_{v,1} - \Re_{v,2}\right) \tag{20}$$

$$S_{m,3} = \frac{M_3}{M_C}\left[\frac{2\alpha}{\alpha+2\beta}\Re_{v,1} + 2\Re_{v,2}\right] \tag{21}$$

$$S_{m,4} = 0 \tag{22}$$

The source of heat in Eq. (2), $\sum S_{h,j}$ is the sum of the enthalpies of the combustion (j = 1) and gasification (j = 2) reactions,

$$\sum S_{h,j} = \Re_{v,1}\Delta H_1 + \Re_{v,2}\Delta H_2 \tag{23}$$

Table 1 lists the kinetic parameters for the char reactions.

Table 1 Kinetic parameters for chemical reactions

Name	Value	Unit	Application	Source
A_{CO/CO_2}	2512	-	$790K \le T_p \le 1690K$	[28]
E_{CO/CO_2}	51.88	kJ/mol	$790K \le T_p \le 1690K$	[28]
$A_{kin,1}$	140	kg/$(m^2 \cdot s)$	AC−char	[34]
$E_{kin,1}$	99	kJ/mol	AC−char	[34]
$A_{kin,2}$	1.67×10^4	kg/$(m^2 \cdot s)$	AC−char	[34]
$E_{kin,2}$	157	kJ/mol	AC−char	[34]
$A_{kin,1}$	10	kg/$(m^2 \cdot s)$	BC−char	[34]
$E_{kin,1}$	58	kJ/mol	BC−char	[34]
$A_{kin,2}$	3.8×10^3	kg/$(m^2 \cdot s)$	BC−char	[34]
$E_{kin,2}$	120	kJ/mol	BC−char	[34]
$A_{kin,1}$	9.5×10^3	kg/$(m^2 \cdot s)$	SBC−char	[34]
$E_{kin,1}$	108	kJ/mol	SBC−char	[34]
$A_{kin,2}$	7.5×10^5	kg/$(m^2 \cdot s)$	SBC−char	[34]
$E_{kin,2}$	148	kJ/mol	SBC−char	[34]
$A_{kin,1}$	35	kg/$(m^2 \cdot s)$	LC−char	[30]
$E_{kin,1}$	181	kJ/mol	LC−char	[30]
$A_{kin,2}$	4.4×10^3	kg/$(m^2 \cdot s)$	LC−char	[30]
$E_{kin,2}$	248	kJ/mol	LC−char	[30]
ΔH_1	$-(\frac{2\alpha}{\alpha+2\beta}\cdot 9.2\times10^3 + (\frac{2\beta}{\alpha+2\beta}\cdot 3.273\times10^4))$	kJ/kg		[35]
ΔH_2	1.439×10^4	kJ/kg		[36]
s_0	1.0×10^5	m^2/m^3	AC−char	[37]
s_0	2.0×10^5	m^2/m^3	BC−char	[37]
s_0	3.0×10^5	m^2/m^3	SBC−char	[38]
s_0	1.5×10^6	m^2/m^3	LC−char	[37]
Ψ	2.5	-	coal−char	[32][33]

2.3 Physico-chemical parameters for the model

The parameters used in the present model are summarized in Tab. 2. The coal particles were carved to a nearly spherical form [12] and it was experimentally verified that the coal particles (for all types investigated in [13]) kept their skeleton during conversion, and so, roughly its initial spherical shape and size. The bulk density of the pyrolyzed chars was estimated by multiplying the percentage of the carbon and ash mass contents with the density of the raw fuels determined experimentally. Gan et al. [39] measured the porosity of different ranks of coal (AC to LC) and found that for most tested coals it was approximately 0.1, so the same porosity was assumed here. The initial porosity of the char ($\varepsilon_{p,0}$) calculated from the changed densities of the char (see Tab. 2), agrees well with the corresponding data on raw coal given in [40]-[42].

Table 2 Parameters of the model

Name	Value	Unit	Application	Source
d_p	6	mm	fuel	[13]
d_b	0.3	mm	bed	[13]
$\rho_{p,0}$	1370	kg/m^3	AC	[12]
$\rho_{p,0}$	1380	kg/m^3	BC	[12]
$\rho_{p,0}$	1230	kg/m^3	SBC	[12]
$\rho_{p,0}$	680	kg/m^3	LC	[12]
ρ_b	2600	kg/m^3	quartz sand	-
$\varepsilon_{p,0}$	0.18	-	AC	[12]
$\varepsilon_{p,0}$	0.21	-	BC	[12]
$\varepsilon_{p,0}$	0.34	-	SBC	[12]
$\varepsilon_{p,0}$	0.59	-	LC	[12]
ε_a	0.85	-	coal−char	[43]
ε_p	$\varepsilon_{p,0}+(\varepsilon_a-\varepsilon_{p,0})X_C$	-	coal−char	[44]
c_p	$1458(1-\varepsilon_p)$	$J/(kg\cdot K)$	coal−char	[44]
λ_p	$1.891(1-\varepsilon_p)^2$	$W/(m\cdot K)$	coal−char	[44]
ω	0.85	-	coal−char	[44]
D_{1k}	$2.2\times10^{-4}(T_p/1023)^{1.75}$ (O_2)	m^2/s	in N_2	[45][46]
D_{2k}	$2.2\times10^{-4}(T_p/1023)^{1.75}$ (CO)	m^2/s	in N_2	[45][46]
D_{3k}	$1.65\times10^{-4}(T_p/1023)^{1.75}$ (CO_2)	m^2/s	in N_2	[45][46]
D_{1k}	$1.7\times10^{-4}(T_p/1023)^{1.75}$ (O_2)	m^2/s	in CO_2	[45][46]
D_{2k}	$1.7\times10^{-4}(T_p/1023)^{1.75}$ (CO)	m^2/s	in CO_2	[45][46]
u_f	0.28	m/s	bed	[13]
ε_{mf}	0.4	-	bed	-

2.4 Numerical solution

An implicit integral−finite volume method [47] was employed to solve the conservation equations with their initial and boundary conditions. The discretized equation of each grid point is presented as a set of linear algebraic equations for a control volume through the central difference method. An integrated C++ code was developed to solve the discretized equations using the Tri−Diagonal Matrix Algorithm with the convergence

criterion of 10^{-3}. To obtain grid and time−step independence, the fuel particle was divided into 300 cells in the radial direction, and the time−step was 1×10^{-6} s.

3. Results and discussion

3.1 Comparison of model results with experiments

The experimental data of char combustion measured by the present authors [13] and data reported in other publications [17]-[20] are compared with the results predicted by the proposed char conversion model. The experimental data were obtained using various techniques under different operational conditions, covering a variety of coal ranks. Table 3 gives the outline of each operation.

1

Table 3 Experimental conditions for studying coal combustion

Reference	Reactor type	Reactor dimension, mm	Operation condition	Measurement	Fuel, particle size, mm	Observations
[13]	FB	200 × 20 × 400	T_b = 1088 K, u/u_{mf} = 1.8, O_2/CO_2 and O_2/N_2, O_2 : 10, 21, 30, 40 $\%_{vol}$.	thermocouple, CCD camera.	AC, BC, SBC, LC, d_p = 6,d_b=0.3	particle temperature, ignition delay time, devolatilization time, burnout time.
[17]	FB	100 (diameter) × 450	T_b = 1023, 1173 K, u/u_{mf} = 2.3, O_2/N_2, O_2 : 2, 5, 8 $\%_{vol}$.	camera, mass balance.	LC, d_p = 1.65−3.28, d_b=0.2	particle mass, devolatilization time, burnout time.
[18]	Convective flow furnace	80 (diameter) × 150	T_r = 900−1200 K, Re_p = 63−126, O_2/N_2, O_2 : 4.5−21 $\%_{vol}$.	mass balance.	BC, SBC, LC, d_p = 5.3−9.9.	particle mass, ignition delay time, devolatilization time, burnout time.
[19]	FB	80 (diameter) × 600	T_b = 863, 983 K, u/u_{mf} = 2.3−3.5, air.	thermocouple, gas analyzer.	LC, d_p = 5-10, d_b=0.25	particle temperature, gas concentration.
[20]	FB	120 (diameter) × 1700	T_b = 1130−1200 K, u = 0.75 m/s, O_2/N_2, O_2 : 5−8 $\%_{vol}$.	fiber−optic two−color optical pyrometry, gas analyzer.	SBC, d_p = 2, d_b=1.6	particle temperature, gas concentration.

2

In our experiments [13], the temperatures of the particle center and ‘ surface’ (there was a 1 mm gap between the thermocouple and the particle surface) were measured continuously during the conversion process. Figure 1 compares the evolution of measured and predicted center and surface temperatures with time of LC particles in O_2/N_2 and O_2/CO_2 at different O_2 levels (only the temperatures higher than 800 K are plotted, the evolution of temperature lower than 800 K (the period of devolatilization) was presented and discussed in previous work [14]). The predictions match reasonably well the measurements, although the particle’ s center temperature is overestimated at the final stage of conversion, which is particularly notable at the highest O_2 concentration. This overestimation probably originates from the physico-chemical parameters establishing the evolution of heat transfer properties with time, especially the correlations used to predict their variation with conversion during the last stages [47]-[49]. For future work, measuring the structure properties of the char particles as a function of the conversion stage, would improve the present heat transport model.

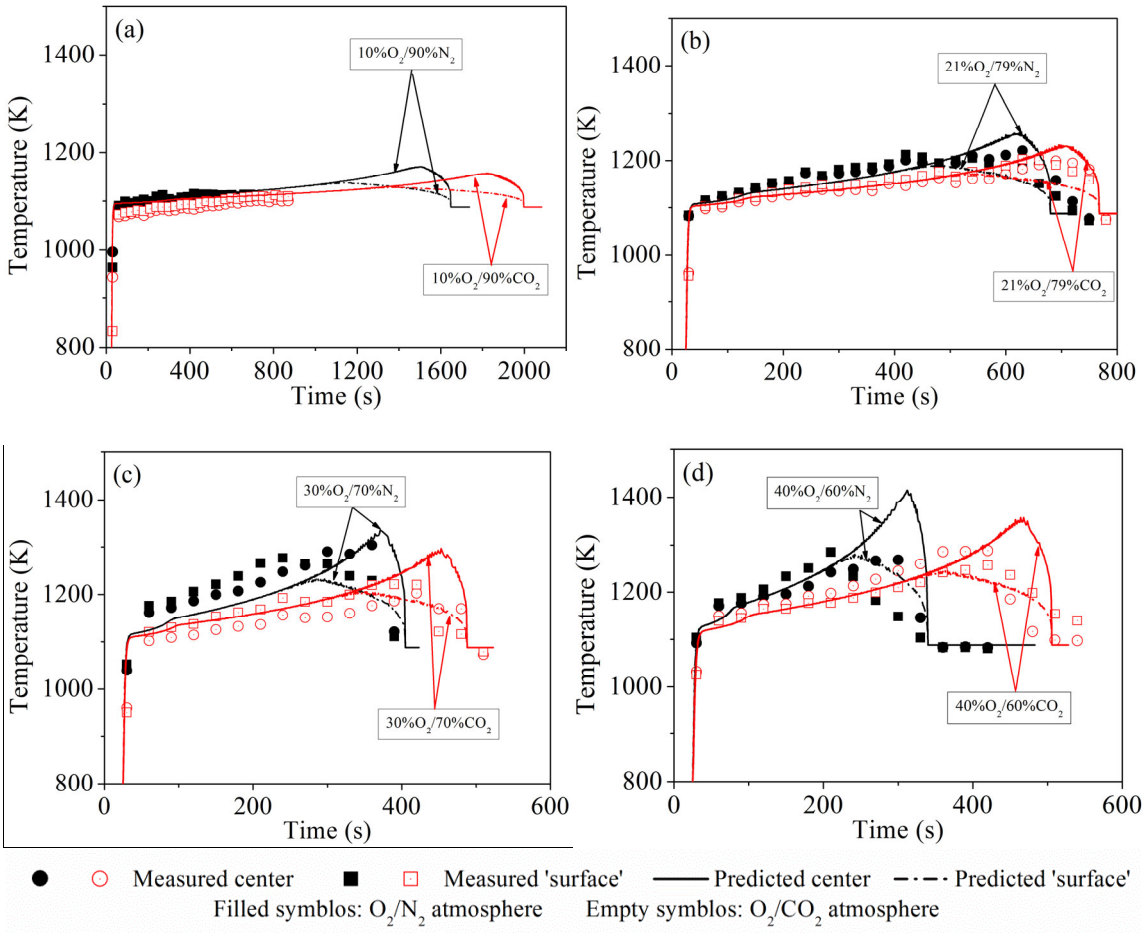

Fig. 1 Comparison of the evolution with time of measured [13] and predicted center and surface temperatures of an LC particle in O_2/N_2 and O_2/CO_2, (a) 10 $\%_{vol}$ O_2, (b) 21 $\%_{vol}$ O_2, (c) 30 $\%_{vol}$ O_2, (d) 40 $\%_{vol}$ O_2. $d_p = 6$ mm, $T_b = 1088$ K, $u/u_{mf} = 1.8$. (Note the different horizontal scales.)

The predicted evolution of the temperature with time for other coal chars (AC, BC, SBC) was also examined and summarized in Fig. 2, which presents the time-history profiles for AC, BC, SBC at $30\%O_2/70\%CO_2$. In the figure, the predicted and measured surface and center temperatures of the particle increase simultaneously with the char conversion until a certain temperature, at which the surface temperature starts decreasing steadily, whereas the center temperature keeps increasing until the attainment of the peak temperature, and then it falls to the bed temperature. This behavior of the particle temperature suggests a combustion mode typical of a coarse particle, where a reaction front moves gradually from the surface to the interior of the particle, while the fuel particle remains at constant size. Figure 5 explains this conversion behavior in detail in the light of the calculated internal species, temperature, and conversion profiles.

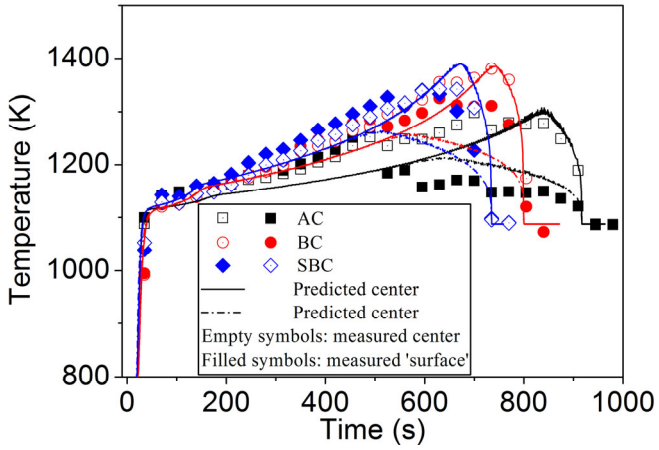

Fig. 2 Comparison of the evolution with time of measured [13] and predicted center and surface temperatures of AC, BC and SBC particles in $30\%O_2/70\%CO_2$, $d_p = 6$ mm, $T_b = 1088$ K, $u/u_{mf} = 1.8$.

Two important conversion characteristics of a fuel particle in an FB are obtained from the temperature history of the particle [13][17][18] and from the gas profile at the outlet of the reactor [19][20]: the burnout time and the peak temperature of the particle [50]. The peak temperature is the maximum temperature of the char particle during its conversion. The burnout time is the period of time from the coal addition to the time at which the difference of temperature between the particle center and the bed is 1 % (after having passed the peak temperature) or to the moment when the measured O_2 concentration at the outlet of the reactor is 99.9% of the inlet value. Figure 3 compares both predicted parameters with the measured ones, showing that the model

predicts reasonably well the burnout time and the peak temperature, since 90% of the experimental data points are within ±15 % and ±20 % deviation, respectively.

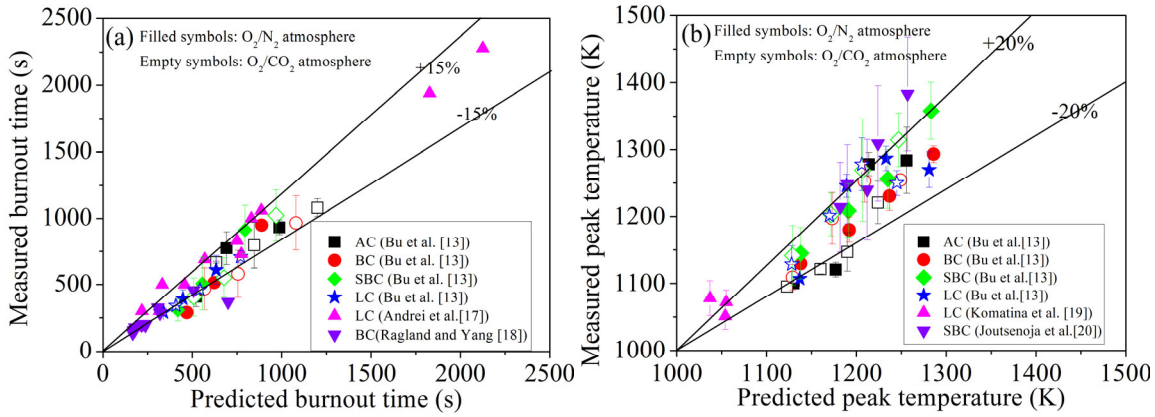

Fig. 3 Comparison of measured [13][17]-[20] and predicted burnout times (a) and peak temperatures (b) under various conditions. The error bars represent the standard deviation. Background data are summarized in Tab. 3.

3.2 Analysis and interpretation of the behavior of char with the model

The main objective of the present work is to quantitatively examine the role of diffusion of O_2 and gasification during conversion of coarse char particles in O_2/CO_2. Here, the LC particle is selected as a fuel for the analysis of these factors. Simulated results of the evolution of the surface temperature with time and the degree of carbon conversion of a 6 mm char particle at 10 and 40 $\%_{vol}$ O_2 concentrations and 1088 K are shown in Fig. 4 for both O_2/N_2 and O_2/CO_2. The gasification reaction is turned on and off in the model to assess its effect in O_2/CO_2.

Figure 4(a), comparing the computed particle surface temperatures in O_2/N_2 and O_2/CO_2 (without gasification) in 10 $\%_{vol}$ and 40 $\%_{vol}$ O_2 concentrations, shows that the decrease of the particle' s heating rate is notable in O_2/CO_2. This is due to the lower diffusivity of O_2 in CO_2 than in N_2, resulting in lower combustion rate, and consequently, lower heat release in O_2/CO_2 conditions. When the gasification reaction is accounted for in the calculation of carbon consumption in the O_2/CO_2 atmosphere, the heating rate of the particle almost does not change, meaning that the endothermic gasification reaction has a very small effect on the particle temperature. The negligible influence of gasification is confirmed by comparing the conversion vs time with and without the gasification reaction in $10\%O_2/90\%CO_2$ and $40\%O_2/60\%CO_2$ in Fig. 4(b). Due to the low combustion rate of char in O_2/CO_2, Fig. 4(b) shows that the burnout time is prolonged by 300 s (without

gasification) in 10%O_2/90%CO_2 compared to that in 10%O_2/90%N_2, and the time is only shortened by 20 s when the gasification reaction is included in the model.

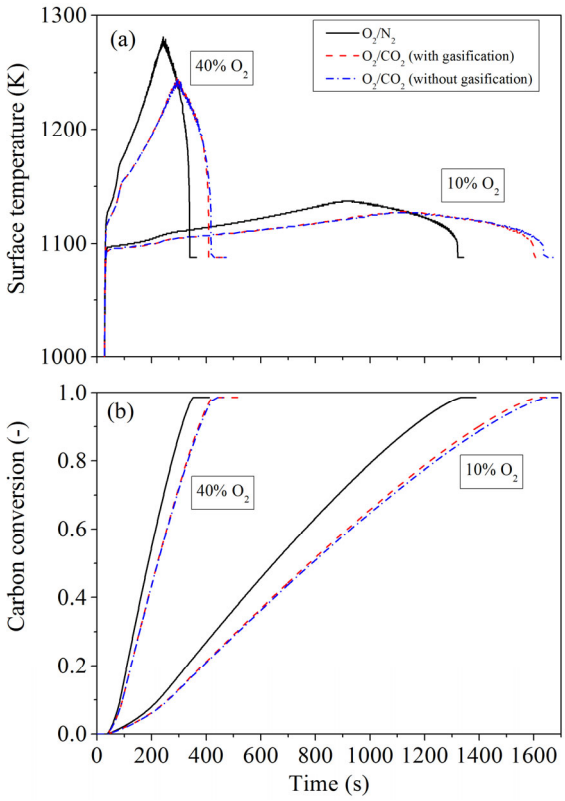

Fig. 4 Simulated evolution with time of the surface temperature of the LC particle (a) and the carbon conversion in O_2/N_2 and O_2/CO_2 (with and without gasification) (b) at 10 and 40 $\%_{vol}$ O_2 concentrations, $d_p =$ 6 mm, $T_b = 1088$ K.

In order to get a deeper insight into the char conversion in O_2/N_2 and O_2/CO_2, the radial profiles of temperature, local carbon conversion (x_C), as well as O_2 and CO_2 mass fractions, are plotted in Fig. 5 as a function of the overall carbon conversion (X_C) for LC at 10 $\%_{vol}$ O_2 concentration (the gas−film δ_h is approximately 1.5 mm, quantified by assuming the film theory, i.e. $\delta_h = d_p/(Nu - 2)$ [51]). Figure 5(a) points out that the particle temperatures are higher in O_2/N_2 than in O_2/CO_2, due to the slower combustion rate in the latter, although similar temperature trends are established in both atmospheres. Figure 5(b) reveals that there is a front of reaction, visualized by the change in local conversion, going from zero to unity in a short reaction thickness (front), which advances inwards leaving behind an ash layer, whose thickness increases with conversion. As seen in Fig.5 (a) the temperature is uniform in the unreacted core (to the left of the reaction front), whereas it drops from the core to the surface throughout the ash layer, and with a negligible gradient in

the gas film. This thermal profile is explained by the lower thermal conductivity of the ash compared to that of the fresh char (the core). This demonstrates that the peak temperature in the particle is governed by the thermal conductivity of the ash (whose thickness increases with time, and so does its resistance to heat transport).

The insignificant contribution of gasification to the overall carbon converted in the char is further confirmed by noting the negligible difference between the profiles marked with filled ($10\%O_2/90\%N_2$) and empty symbols ($10\%O_2/90\%CO_2$) for a given degree of total carbon conversion (X_C).

Figure 5(c) shows that, at the initial stage of the carbon conversion ($X_C = 0.05$), the oxygen concentration drops to zero in the external layer of the gas film and the reaction front is located at the particle' s surface in both O_2/CO_2 and O_2/N_2 (filled vs empty symbols). As reaction proceeds, the reaction front moves into the particle and the gradients of the O_2 concentration become significant in the ash−layer too. At high conversion ($X_C = 0.95$) the combustion process is controlled by O_2 diffusion both in the porous ash−layer and in the gas−film.

Figure 5(d) shows that the CO_2 concentration at the reaction front is a little bit higher than in the bulk gas both in O_2/CO_2 and O_2/N_2, indicating that the amount of CO_2 released from the combustion (Reaction R1) is larger than that consumed by gasification (Reaction R2).

The analysis of Fig. 5 was made for $10\%O_2$, i.e. $10\%O_2/90\%N_2$ and $10\%O_2/90\%CO_2$, but similar behavior was verified for other $\%O_2$ both in N_2 and CO_2 atmospheres.

Overall, the rate of conversion of char particles, and so the conversion time and peak temperature, during FB combustion both in O_2/CO_2 and O_2/N_2 is governed by the rate of transport of O_2 in the external gas−film and ash layer as well as by the heat transport through the ash layer formed during conversion. This behavior allows simplification of the model developed in the previous section by considering only these main resistances. The resulting model is the so-called non−isothermal sharp interface model (SIM) [52], providing analytical solutions for the burnout time and peak temperature. The application of SIM can be very useful to simplify computational fluid-dynamics (CFD) simulations of char combustion in FB.

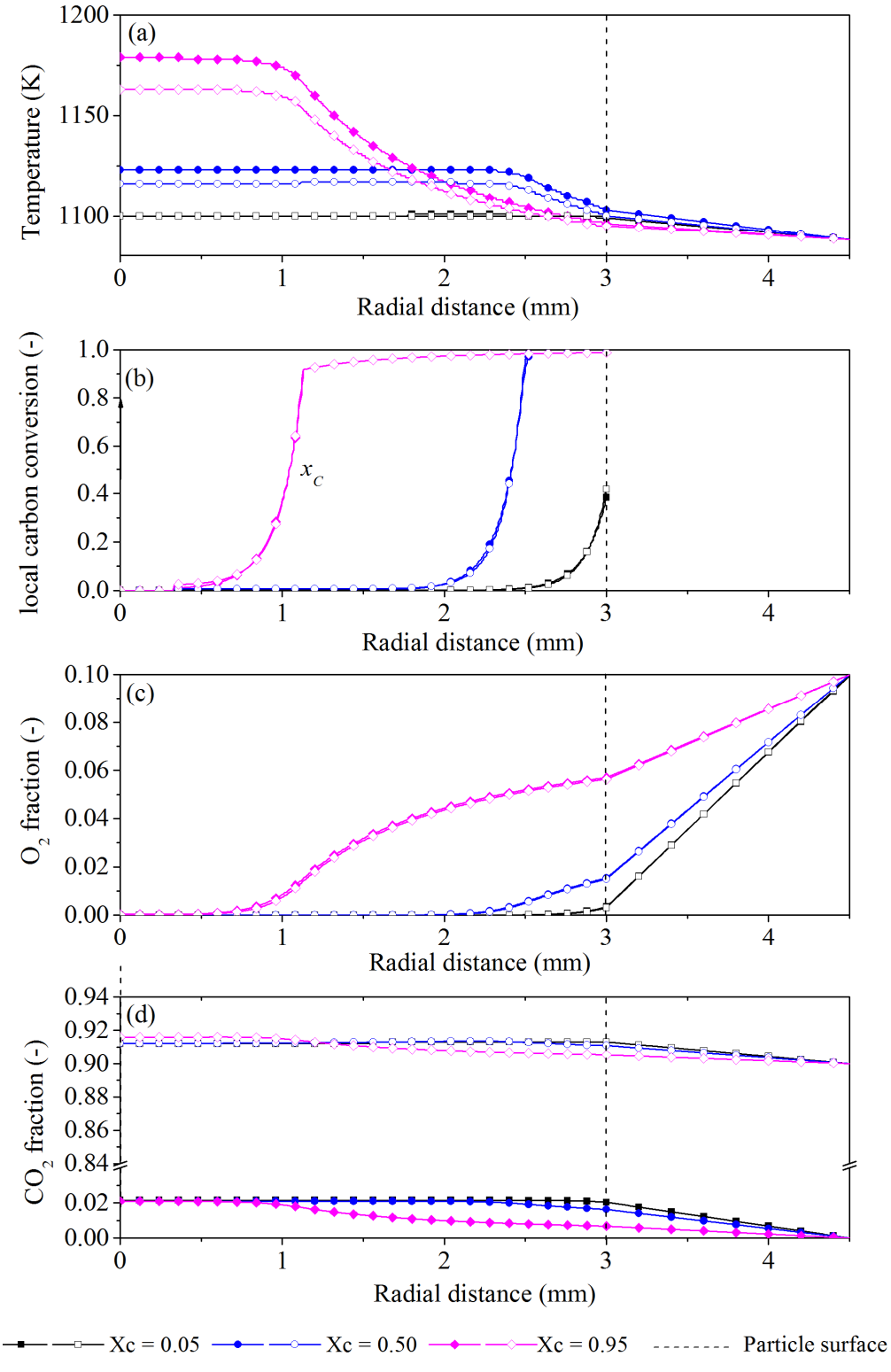

Fig. 5 Simulated particle temperature (a), local carbon conversion (x_C) (b), O_2 fraction (c), CO_2 fraction (d) along the radius at different degrees of total carbon (X_C) conversion in O_2/N_2 and O_2/CO_2 for 10 $\%_{vol}$ O_2 concentration, LC particle $d_p = 6$ mm, $T_b = 1088$ K.

3.3 Sensitivity analysis: influence of model parameters

Several input parameters were estimated in the model, such as initial properties of the char, including thermal conductivity of the particle $(\lambda_{p,0})$, particle porosity $(\varepsilon_{p,0})$, particle thermal capacity $(c_{p,0})$ and particle density $(\rho_{p,0})$, the effective particle-gas heat and mass transfer coefficients $(h_{\mathrm{h,eff}}, h_{m,i})$, and the reactivity of gasification$(\Re_{v,2})$. A sensitivity analysis was carried out to study the relative influence of these factors on the burnout time and the peak surface temperature of the particle. Figure 6 shows the results obtained by decreasing and increasing one parameter at the time by 30 %, with the exception of $\Re_{v,2}$, while maintaining the other parameters constant, for an LC particle in 10%O_2/90%CO_2. The sensitivity of the gasification reaction rate is investigated by decreasing and increasing $\Re_{v,2}$ one order of magnitude, because this variation takes into account the differences between the char gasification kinetics reported in the literature.

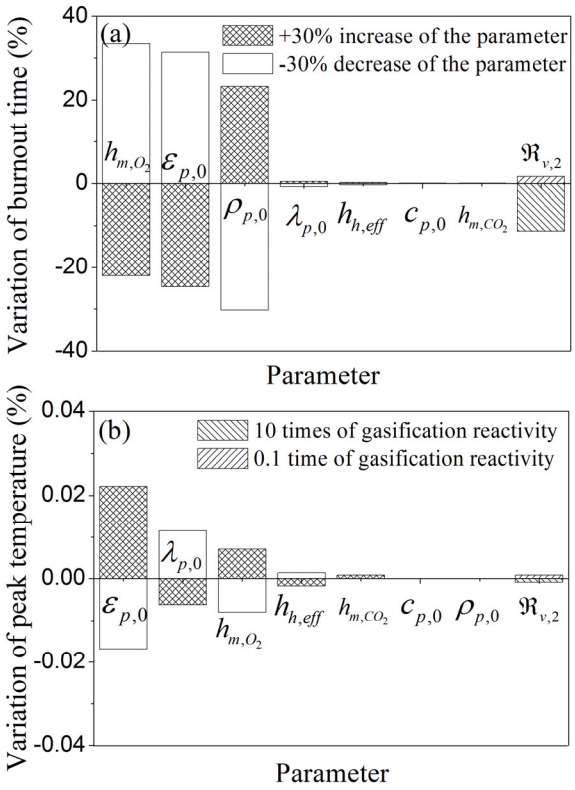

Fig. 6 Sensitivity analysis of the model parameters, (a) variation of the burnout time and (b) variation of the peak surface temperature. LC, $d_p = 6$ mm, $T_b = 1088$ K, 10%O_2/90%CO_2. (Note the different vertical scales.)

As shown in Fig. 6(a), h_{m,O_2}, $\varepsilon_{p,0}$, and $\rho_{p,0}$ are three main parameters influencing the burnout time, which apparently decreases with the increase of h_{m,O_2} and $\varepsilon_{p,0}$, but with a decrease of $\rho_{p,0}$. The parameters $\lambda_{p,0}$,

$h_{\mathrm{h,eff}}$, $c_{p,0}$, and h_{m,CO_2} have a very limited effect on the burnout time of the fuel particle. Thus, the longer burnout time in O_2/CO_2 than in O_2/N_2 for a given coal, observed in experiments [13], is mainly attributed to the lower h_{m,O_2} in CO_2 as compared to N_2. The lower the rank of coal, the higher is $\varepsilon_{p,0}$ and the lower $\lambda_{p,0}$, leading to shorter burnout time. Meanwhile, Figure 6(b) shows that $\varepsilon_{p,0}$, $\lambda_{p,0}$ and h_{m,O_2} are the major factors affecting the peak temperature of the particle. The small variation of the peak temperature with the change of $h_{\mathrm{h,eff}}$, $c_{p,0}$, $\rho_{p,0}$, and h_{m,CO_2} explains the similar peak temperatures measured for the different types of fuel in $10\%O_2/90\%N_2$ and $10\%O_2/90\%CO_2$ [13].

The decrease of $\Re_{v,2}$ by ten times has a minimal impact on burnout time and peak temperature, (Fig. 6), which was expected, since the rate of the gasification reaction was slow already in the base case. However, 10 times magnification of $\Re_{v,2}$ decreases the burnout time by 10% (which is still within the accuracy of the developed model), whereas the peak temperature does not change much. Several cases with even 100 times higher $\Re_{v,2}$ were also simulated, but the evolution of the predicted particle temperature with time was not consistent with the measurements, so that it is not presented in Fig. 6. In addition, since the gasification reactivity decreases with the rank of the coal, the sensitivity analysis of $\Re_{v,2}$ made for LC (which has the highest reactivity), enables extending the conclusions to other ranks of coal tested in the experiments presented in [13].

3.4 Influence of operating conditions on oxy-fuel FB boiler operation

In the present work, extended simulations in O_2/CO_2, including comparison with O_2/N_2, are carried out in order to study the combustion behavior of the char in a commercial FB supplying some basics data and information for the effective implementation of oxy-fuel FB. In a commercial FB combustor, char particles could be exposed on an average to 3−7 $\%_{\mathrm{vol}}$ O_2 with a particle size ranging from 1 to 10 mm at bed temperatures of 1073 to 1173 K [53]. In this section, although only LC is adopted for further analysis, most results can be generalized to other ranks of fuel.

3.4.1 Effect of O_2 concentration

Figure 7(a) presents the simulated evolution of the peak surface temperature (T_{peak}) and burnout time (t_{burn}) of the LC in O_2/N_2 and O_2/CO_2 at O_2 concentrations from 5 to 60 $\%_{\mathrm{vol}}$ at 1088 K with the particle size (d_p) of 6 mm. The experimental data points of LC measured in our previous work [13] are also plotted. The burnout time t_{burn} decreases with the increase of O_2 concentration both in O_2/N_2 and O_2/CO_2, and the simulated trend of the t_{burn} with O_2 concentration fits well the experiments. Besides, it is noticed that the decrease of

burnout time with O_2 levels off at high % O_2 because the O_2 mass diffusion (both in the gas film and ash layer) controls the combustion process and the driving force of O_2 decreases at high O_2 concentration as a consequence of its low diffusivity in the ash layer. The simulated T_{peak} reflects qualitatively the increasing tendency with O_2 concentration that was also detected in the measurements. Simulations predict a linear increase of the peak temperature, whereas the measured T_{peak} levels off at high O_2 concentration. This is consistent with the failure of the model at high conversion (where the peak temperature is reached) as was discussed in connection to Fig. 1.

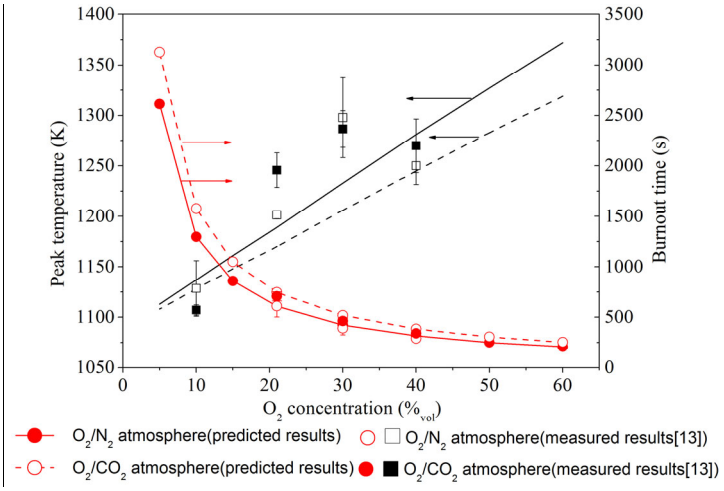

(a) the peak surface temperature and the burnout time

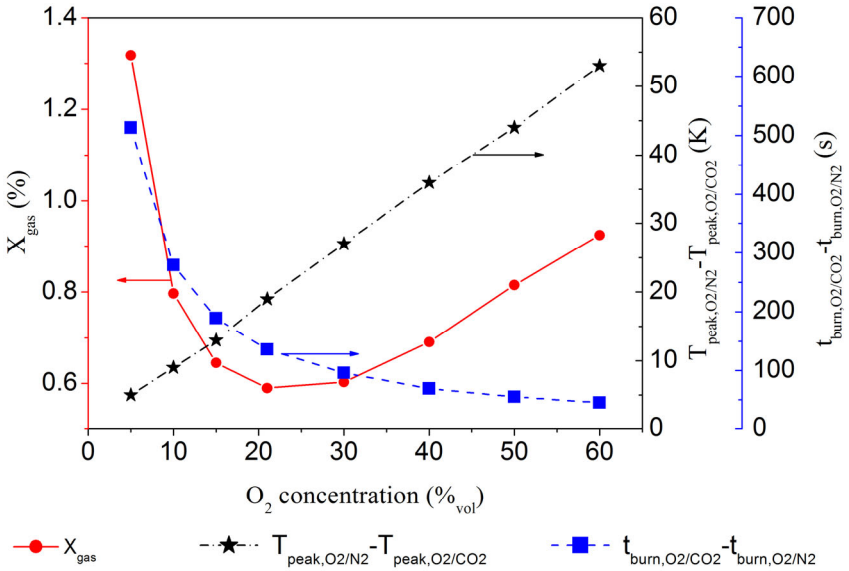

(b) the percentage of LC char consumed by CO_2 gasification (X_{gas}) in O_2/CO_2; the peak surface temperature difference ($T_{peak,N_2} - T_{peak,CO_2}$) and the burnout time difference ($t_{burn,CO_2} - t_{burn,N_2}$)

Figure 7 Simulated results of the effect of O_2 concentrations on LC combustion characteristics. $d_p = 6$ mm, $T_b = 1088$ K.

To assess the effect of CO_2 on char conversion and the role of gasification, the percentage contribution of CO_2-char gasification to the consumption of LC char (X_{gas}) in the oxy−fuel mode, the peak surface temperature difference ($T_{peak,N_2} - T_{peak,CO_2}$), and the burnout time difference ($t_{burn,CO_2} - t_{burn,N_2}$) for O_2/CO_2 and O_2/N_2 are plotted in Fig. 7(b) under the same condition as in Fig. 7(a). The contribution of gasification (X_{gas}) is only 0.6−1.3 % of the total char converted. As the O_2 concentration increases, X_{gas} decreases until reaching a minimum value of 0.6% at 21 $\%_{vol}$ O_2, and then it increases again due to the transition of the ratio of the increased particle temperature to the decreased CO_2 concentration [5], in agreement with previous measurements [6]. It was concluded from the analysis made before that the peak temperature of the particle in O_2/CO_2 is always lower than that in O_2/N_2 for the same $\%O_2$, so the difference between the two peak temperatures is positive. In Fig. 7(b) this difference is plotted as a function of O_2, showing that not only the difference is positive, but that the difference increases linearly with O_2, which is consistent with the negligible contribution of gasification to the carbon converted. From 5 to 20 $\%_{vol}$ O_2, the difference of the burnout time decreases rapidly from 560 s to 140 s. With further increase of the O_2, the difference in burnout time decreases gradually because the mass transfer of O_2 controls the combustion process of the char particle as mentioned before.

3.4.2 Effect of coal particle size

The evolution of the calculated T_{peak} and t_{burn} of LC with particle diameter in $5\%O_2/95\%N_2$ and $5\%O_2/90\%CO_2$ at 1088 K is plotted in Fig. 8(a). The larger the particle size, the longer the predicted t_{burn}. The peak temperature T_{peak} increases with particle size mainly due to the decreased heat-transfer coefficient.

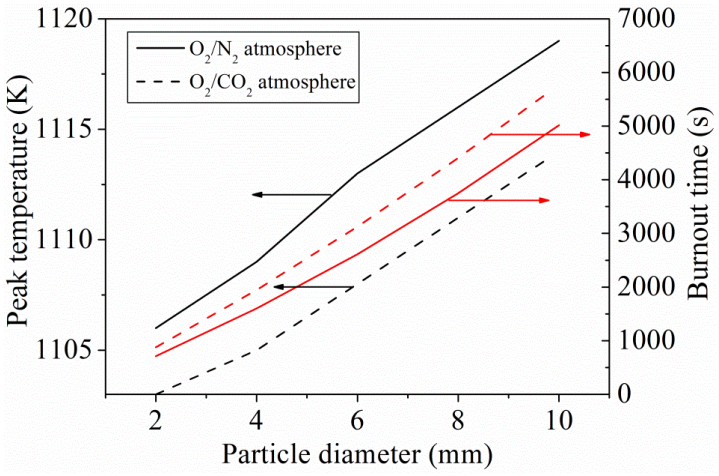

(a) the peak surface temperature and the burnout time

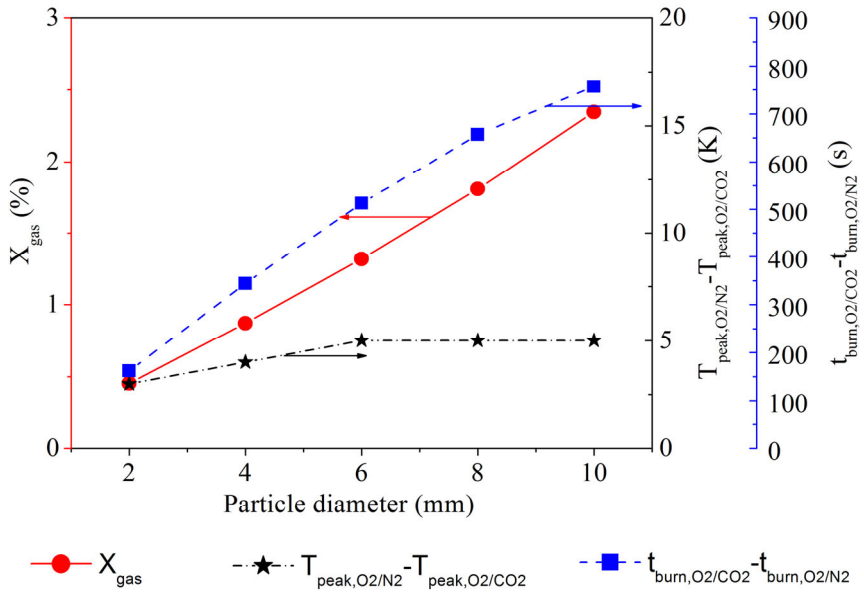

(b) the percentage of LC char consumed by CO_2 gasification (X_{gas}) in O_2/CO_2; the peak surface temperature difference ($T_{peak,N_2} - T_{peak,CO_2}$) and the burnout time difference ($t_{burn,CO_2} - t_{burn,N_2}$)

Figure 8 Simulated results of the effect of particle size on LC combustion characteristics. O_2 concentration 5%, $T_b = 1088$ K.

Figure 8(b) shows the evolution with particle size of X_{gas}, ($t_{burn,CO_2} - t_{burn,N_2}$), and ($T_{peak,N_2} - T_{peak,CO_2}$) of an LC particle. X_{gas} increases with the particle size to its maximal value of 2.3% at 10 mm due to the increased burnout time and particle temperature. Because O_2 diffusion controls the combustion process, the relative burnout time difference ($t_{burn,CO_2} - t_{burn,N_2}$) between O_2/CO_2 and O_2/N_2 increases with the particle size, attaining a maximum value of 750 s. The peak temperature difference ($T_{peak,N_2} - T_{peak,CO_2}$) of the particle does not change much (5 K) with the particle size, because the peak temperature is controlled by the thermal conductivities of char and ash, and it is insignificantly influenced by the different atmospheres (note that the peak temperature increases during the increase of the particle size from 6 to 10 mm, as shown in Fig. 8a).

3.4.3 Effect of bed temperature

Figure 9(a) shows how T_{peak} increases and t_{burn} decreases with the bed temperature (T_b) for 6 mm LC-char particles in 5%O_2/95%N_2 and 5%O_2/90%CO_2. The tendencies of t_{burn} are not the same in O_2/N_2 as in O_2/CO_2. In O_2/N_2, the combustion process is mainly controlled by O_2 diffusion, which is hardly sensitive to temperature. However, when N_2 is replaced by CO_2, gasification accounts for a significant part of the total

carbon consumed in the char (at high temperature) and then t_{burn} is also influenced by the rate of gasification. At low bed temperature, the rate of gasification is so low that its influence on t_{burn} is negligible. However, the sensitivity of the gasification reaction is high (high activation energy), and a further increase of temperature results in a significant reduction of t_{burn}. As seen by the shaded region in Fig. 9(a), at bed temperatures above 1173 K, the burnout time in O_2/CO_2 decreases below the value in O_2/N_2. This is in the upper range of feasible operation temperature of a commercial FBC boiler.

The evolution of X_{gas}, $t_{burn,CO_2} - t_{burn,N_2}$, and $T_{peak,N_2} - T_{peak,CO_2}$ of an LC particle ($d_p = 6$ mm) with bed temperature is plotted in Fig. 9(b). As expected, the higher the bed temperature, the larger is the contribution of gasification, X_{gas}. Consequently, as shown in Fig. 9(b), $t_{burn,CO_2} - t_{burn,N_2}$ and $T_{peak,N_2} - T_{peak,CO_2}$ decrease with the bed temperature because of the enhanced carbon conversion by gasification, consuming heat. When the bed temperature attains 1223 K, X_{gas} is 14 % and cannot be ignored, the peak temperature in O_2/CO_2 is higher and the burnout time shorter than in O_2/N_2. This combustion behavior has been experimentally confirmed by Saucedo et al. [54] using an LC in FB. X_{gas} is much smaller at the commercial operation temperature of the FB (see the shaded region in Fig. 9(b)). For other coal ranks X_{gas} is even less, because the gasification reactivity decreases with coal rank.

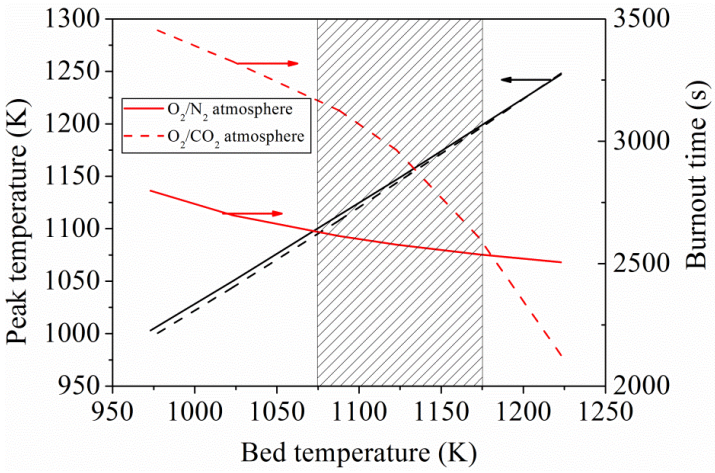

(a) the peak surface temperature and the burnout time

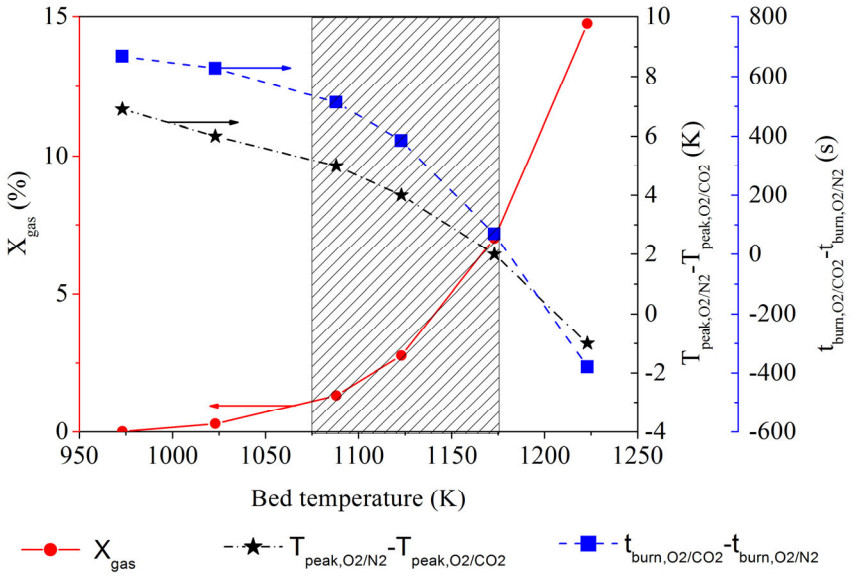

(b) the percentage of LC char consumed by CO_2 gasification (X_{gas}) in O_2/CO_2; the peak surface temperature difference ($T_{peak,N_2} - T_{peak,CO_2}$) and the burnout time difference ($t_{burn,CO_2} - t_{burn,N_2}$)

Figure 9 Simulated results of the effect of bed temperature on LC combustion characteristics. O_2 concentration 5%, $d_p = 6$ mm. The shaded region represents results under commercial FB combustor conditions.

Overall, when O_2/N_2 is replaced by O_2/CO_2, the O_2 concentration, the particle size, and the bed temperature have notable effects on the burnout time of a char particle; for the peak temperature, the O_2 concentration and the bed temperature show a larger influence than that of the particle size; the CO_2 gasification is mainly affected by the bed temperature, whereas the changes in the O_2 concentration and the particle size show negligible effects. For retrofit of existing FB boilers, increasing inlet O_2 concentration and the bed temperature in the O_2/CO_2 mode can achieve similar combustion characteristics as in air. However, the efficiency of the FB plant is decreased as result of the increased cost for pure O_2 production. Increasing the bed temperature (e.g. 1173 K) could be a good option which should be further experimentally validated in pilot scale FB.

In addition, in a commercial FB reactor, the bed temperature and the O_2 and CO_2 concentrations around a char particle are not constant during its conversion. Furthermore, the ash layer could be removed from the particle by collision between the particles at high velocity, decreasing the size of the particle. Therefore, T_{peak} and t_{burn} reported in the present work could vary, and further studies are still needed to take these factors into account.

4. Conclusion

A model of a single char particle for oxy-fuel combustion was developed to study the effect of CO_2 in oxy-fuel combustion of coal char-particles in FB. The model was compared with past measurements and showed a good ability to predict the main combustion characteristics of coarse fuel particles in FB, both in O_2/N_2 and O_2/CO_2 atmospheres. The model reproduces the evolution of char temperature with time for various coal types and operating conditions except at the latest stage of conversion, when the existing correlations selected to model the variation of thermal conductivity with the porous structure seem not to be accurate enough. The accuracy of the model for the prediction of the burnout time and the peak temperature is within ±15 % and ± 20 %, respectively.

The model was then used to study the performance of a commercial oxy-fuel FB operating with different O_2 levels, particle sizes, and bed temperatures. These were compared with a conventional air-based FB combustor. The results from the study reveal that:

- The rate of conversion of mm-size char particles, and so the conversion time and peak temperature, during FB combustion, both in O_2/CO_2 and O_2/N_2, is governed by the rate of transport of O_2 in the external gas−film and within the ash layer formed, as well as by the rate of heat flow through this ash layer. The difference between combustion in O_2/N_2 and O_2/CO_2 is essentially due to the lower O_2 diffusion rate in CO_2 than that in N_2.
- The effect of gasification on the char particle-temperature and the burn-out times is limited at the usual bed temperature of FB boilers (up to 1173 K), but it shows a considerable effect on the burnout time at higher bed temperature (above 1223 K).
- Sensitivity analysis using the model showed that the diffusivity of O_2, porosity, thermal conductivity, and density of the fuel particle are the main parameters influencing the rate of combustion of the fuel particle, explaining the experimental findings found in the previous part of this work [13].
- The conversion of char under the conditions investigated could be reasonably well described by a simplified version of the model developed here, the so-called non-isothermal sharp-interface model, allowing to greatly simplify the computation in reactor simulations.

Acknowledgements

This work was financially supported by the National Natural Science Foundation of China (No. 51276036), China Postdoctoral Science Foundation (No. 2016M591879) and MICINN (Spain) Project OXYGAS 2G (No.

ENE2012-37999). The support from Chalmers University of Technology (CTH) to two of the authors (C. Bu and A. Gómez-Barea) during their stays at CTH is also acknowledged.

References

[1] Maffei T, Khatami R, Pierucci S, Faravelli T, Ranzi E, Levendi Y A. Experimental and modeling study of single coal particle combustion in O_2/N_2 and Oxy-fuel (O_2/CO_2) atmospheres. Combust. Flame 2013; 160 (11): 2559-2572.

[2] Tolvanen H, Raiko R. An experimental study and numerical modeling of combusting two coal chars in a drop-tube reactor: A comparison between N_2/O_2, CO_2/O_2, and $N_2/CO_2/O_2$ atmospheres. Fuel 2014; 124 (0): 190-201.

[3] Kim D, Choi S, Shaddix CR, Geier M. Effect of CO_2 gasification reaction on char particle combustion in oxy-fuel conditions. Fuel 2014; 120 (0): 130-140.

[4] Prationo W, Zhang J, Abbas HAA, Wu X, Chen X, Zhang L. Influence of External Clay and Inherent Minerals on Lignite Optical Ignition and Volatile Flame Propagation in Air-Firing and Oxy-Firing. Ind. Eng. Chem. Res. 2014; 53 (7): 2594-2604.

[5] Hecht ES, Shaddix CR, Geier M, Molina A, Haynes BS. Effect of CO_2 and steam gasification reactions on the oxy-combustion of pulverized coal char. Combust. Flame 2012; 159 (11): 3437-3447.

[6] Yin C, Yan J. Oxy-fuel combustion of pulverized fuels: Combustion fundamentals and modeling. Appl Energy 2016; 162: 742-762.

[7] Scala F, Chirone R. Combustion of Single Coal Char Particles under Fluidized Bed Oxyfiring Conditions. Ind. Eng. Chem. Res. 2010; 49 (21): 11029-11036.

[8] Duan L, Sun H, Zhao C, Zhou W, Chen X. Coal combustion characteristics on an oxy-fuel circulating fluidized bed combustor with warm flue gas recycle. Fuel 2014; 127 (0): 47-51.

[9] Lupion M, Alvarez I, Otero P, Kuivalainen R, Lantto J, Hotta A, Hack H. 30 MWth CIUDEN Oxy-cfb Boiler - First Experiences. Energy Procedia 2013; 37 (0): 6179-6188.

[10] Brix J, Navascués LG, Nielsen JB, Bonnek PL, Larsen HE, Clausen S, Glarborg P, Jensen AD. Oxy-fuel combustion of millimeter-sized coal char: Particle temperatures and NO formation. Fuel 2013; 106 (0): 72-78.

[11] Roy B, Bhattacharya S. Combustion of single char particles from Victorian brown coal under oxy-fuel fluidized bed conditions. Fuel 2016; 165: 477-483.

[12]Bu C, Leckner B, Chen X, Pallarès D, Liu D, Gómez–Barea A. Devolatilization of a single fuel particle in a fluidized bed under oxy-combustion conditions. Part A: Experimental results. Combust. Flame 2015; 162(3):797-808.

[13]Bu C, Pallarès D, Chen X, Gómez–Barea A, Liu D, Leckner B, Lu P. Oxy–fuel combustion of a single fuel particle in a fluidized bed: Char combustion characteristics, an experimental study. Chem. Eng. J. 2016; 287:649-656.

[14]Chern J S, Hayhurst A N. Fluidised bed studies of:(i) Reaction-fronts inside a coal particle during its pyrolysis or devolatilisation,(ii) the combustion of carbon in various coal chars. Combust. Flame 2015; 159(2): 367-375.

[15]Haseli Y, Van Oijen J A, De Goey L P H. A detailed one-dimensional model of combustion of a woody biomass particle. Bioresour. Technol. 2011; 102(20): 9772-9782.

[16]Bu C, Leckner B, Chen X, Gómez-Barea A, Liu D, Pallarès D. Devolatilization of a single fuel particle in a fluidized bed under oxy–combustion conditions. Part B: Modeling and comparison with measurements. Combust. Flame 2015; 162(3):809-818.

[17]Andrei MA, Sarofim AF, Beér JM. Time-resolved burnout of coal particles in a fluidized bed. Combust. Flame 1985; 61(1): 17-21.

[18]Ragland KW, Yang JT. Combustion of millimeter sized coal particles in convective flow. Combust. Flame 1985; 60(3): 285-297.

[19]Komatina M, Manovic V, Dakic D. An Experimental Study of Temperature of Burning Coal Particle in Fluidized Bed. Energy Fuels 2005; 20(1): 114-119.

[20]Joutsenoja T, Heino P, Hernberg R, Bonn B. Pyrometric temperature and size measurements of burning coal particles in a fluidized bed combustion reactor. Combust. Flame 1999; 118(4): 707-717.

[21]Leckner B, Gómez-Barea A. Oxy-fuel combustion in circulating fluidized bed boilers. Appl Energy 2014; 125, 308 –318

[22]Manovic V, Komatina M, Oka S. Modeling the temperature in coal char particle during fluidized bed combustion. Fuel 2008; 87(6): 905-914.

[23]Laurendeau NM. Heterogeneous kinetics of coal char gasification and combustion. Prog. Energy Combust. Sci. 1978; 4 (4): 221-270.

[24]Yamashita T, Fujii Y, Morozumi Y, Aoki H, Miura T. Modeling of gasification and fragmentation behavior of char particles having complicated structures. Combust. Flame 2006; 146 (1–2): 85-94.

[25]Bird RB, Stewart WE, Lightfoot EN. Transport phenomena. John Wiley & Sons, 2007.Palchonok G. Heat and mass transfer to a single particle in fluidized bed. Phd thesis, Chalmers University of Tecnology, 1998.

[26]Senneca O, Cortese L. Kinetics of coal oxy-combustion by means of different experimental techniques. Fuel 2012; 102(0): 751-759.

[27]Rajan RR, Wen CY. A comprehensive model for fluidized bed coal combustors. AlChE J. 1980; 26(4): 642-655.

[28]Arthur J R. Reactions between carbon and oxygen. Faraday Soc Trans 1951; 47(1):164–178.

[29]Sadhukhan AK, Gupta P, Saha RK. Modeling and experimental studies on single particle coal devolatilization and residual char combustion in fluidized bed. Fuel 2011; 90 (6): 2132-2141.

[30]Kulasekaran S, Linjewile TM, Agarwal PK. Mathematical modeling of fluidized bed combustion 3. Simultaneous combustion of char and combustible gases. Fuel 1999; 78 (4): 403-417.

[31]Bhatia SK, Perlmutter DD. A random pore model for fluid-solid reactions: II. Diffusion and transport effects. AlChE J. 1981; 27 (2): 247-254.

[32]Raghunathan K, Yang RYK. Unification of coal gasification data and its applications. Ind. Eng. Chem. Res. 1989; 28 (5): 518-523.

[33]Wang X, Zeng X, Yang H, Zhao D. General modeling and numerical simulation of the burning characteristics of porous chars. Combust. Flame 2012; 159 (7): 2457-2465.

[34]Gonzalo-Tirado C, Jiménez S, Ballester J. Kinetics of CO_2 gasification for coals of different ranks under oxy-combustion conditions. Combust. Flame 2013; 160: 411–416.

[35]Safronov D, Nikrityuk P, Meyer B. Fixed-grid method for the modelling of unsteady partial oxidation of a spherical coal particle. Combust Thero Model 2011; 16 (4): 589-610.

[36]Dhaneswar SR, Pisupati SV. Oxy-fuel combustion: The effect of coal rank and the role of char-CO_2 reaction. Fuel Process. Technol. 2012; 102 (0): 156-165.

[37]Turnbull E, Kossakowski ER, Davidson JF, Hopes RB, Blackshaw HW, Goodyer PTY. Effect of pressure on combustion of char in fluidised beds. Chem Engng Res Des 1984; 62: 223−234.

[38]Salatino P, Massimilla L. A descriptive model of carbon attrition in the fluidized combustion of a coal char. Chem. Eng. Sci. 1985; 40 (10): 1905-1916.

[39]Gan H, Nandi SP, Walker JPL. Nature of the porosity in American coals. Fuel 1972; 51 (4): 272-277.

[40]Su JL, Perlmutter DD. Effect of pore structure on char oxidation kinetics. AlChE J. 1985; 31(6): 973-981.

[41]Sadhukhan AK, Gupta P, Saha RK. Characterization of porous structure of coal char from a single

devolatilized coal particle: Coal combustion in a fluidized bed. Fuel Process. Technol. 2009; 90(5): 692-700.

[42]Kamishita M, Mahajan OP, Walker JPL. Effect of carbon deposition on porosity and reactivity of a lignite char. Fuel 1977; 56 (4): 444-450.

[43]Mehrabian R, Shiehnejadhesar A, Scharler R, Obernberger I. Multi-physics modelling of packed bed biomass combustion. Fuel 2014; 122 (0): 164-178.

[44]Sotirchos SV, Amundson NR. Dynamic behavior of a porous char particle burning in an oxygen-containing environment: Part I: Constant particle radius. AlChE J. 1984; 30(4): 537-549.

[45]Marek E, Swiatkowski B. Experimental studies of single particle combustion in air and different oxy-fuel atmospheres. Appl Therm Eng 2014; 66: 35-42.

[46]Wang C, Zhang X, Liu Y, Che D. Pyrolysis and combustion characteristics of coals in oxyfuel combustion. Appl Energy 2012; 97: 264–273.

[47]Patankar, SV. Numerical Heat Transfer and Fluid Flow; Hemisphere: New York, 1980.

[48]Chirone R, Massimilla L, Salatino P. Comminution of carbons in fluidized bed combustion. Prog. Energy Combust. Sci.1991; 17 (4):297-326.

[49]Walsh PM, Li T. Fragmentation and attrition of coal char particles undergoing collisions during combustion at temperatures from 900 to 1100 K. Combust. Flame 1994; 99 (3–4):749-757.

[50]Turnbull E, Davidson JF. Fluidized combustion of char and volatiles from coal. AlChE J. 1984; 30(6): 881-889.

[51]Dreybrodt W, Buhmann D. A mass transfer model for dissolution and precipitation of calcite from solutions in turbulent motion. Chem. Geol. 1991; 90 (1–2): 107-122.

[52]Brem G, Brouwers JJH. Analytical solutions for non-linear conversion of a porous solid particle in a gas–II. Non-isothermal conversion and numerical verification. Chem. Eng. Sci. 1990; 45(7): 1915-1924.

[53]Leckner B. Fluidized bed combustion: Mixing and pollutant limitation. Prog. Energy Combust. Sci. 1998; 24(1): 31-61.

[54]Saucedo MA, Butel M, Scott SA, Collings N, Dennis JS. Significance of gasification during oxy-fuel combustion of a lignite char in a fluidised bed using a fast UEGO sensor. Fuel 2015; 144: 423–438.